A new Method for Processing Time Averaged Vibration Patterns
Linear Regression

Somers, P. A A M; Bhattacharya, N.

DOI
10.1111/str.12188

Publication date
2016

Document Version
Accepted author manuscript

Published in
Strain: an international journal for experimental mechanics

Citation (APA)
Somers, P. A. A. M., & Bhattacharya, N. (2016). A new Method for Processing Time Averaged Vibration Patterns: Linear Regression. *Strain: an international journal for experimental mechanics*, *52*(4), 264-275. https://doi.org/10.1111/str.12188

A new method for processing time averaged vibration patterns: linear regression

Running head title: Linear regression for time averaged vibration patterns

Peter A.A.M. Somers and Nandini Bhattacharya
Optics Research Group, Delft University of Technology.
Lorentzweg 1, NL-2628 CJ Delft, the Netherlands
p.a.a.m.somers@tudelft.nl
n.bhattacharya@tudelft.nl

ABSTRACT

Speckle based interferometry systems are useful tools for measuring vibration patterns at harmonically vibrating objects. The standard method for processing the speckle patterns acquired is to eliminate additive background noise and speckle phase, yielding Bessel-type fringe patterns whose values are proportional to the absolute value of the Bessel function. Fringes are covered by multiplicative speckle intensity noise on the Bessel-modulated vibration amplitude. Sine-cosine filtering is not an option since the Bessel-type fringe pattern is not a phase pattern and thus sine-cosine filtering would only degrade the results. Improvements can be reached by involving additional measurements acquired in the stationary state. An alternative method for processing vibration patterns using linear regression is proposed, yielding patterns where the vibration amplitude is an argument of a true Bessel function, not its absolute value. As a result, spatial frequencies of the vibration fringe pattern are only half of those obtained with standard methods, and results can be filtered and normalized conveniently. While other contributions to improve the results rely on determining indexed skeletons for high Bessel fringe densities, the proposed method aims at a very limited number of low-order fringes, allowing demodulation of the Bessel fringe pattern based on the actual Bessel values in the pattern. The method provides an effective alternative for spatial filtering. Phase differences between the stationary and vibrating states have an adverse effect on the results. Two methods, capable of handling phase jumps of 2π in the phase difference distribution, are presented to correct this.

KEYWORDS: linear regression, speckle interferometer, shearography, vibration, time-averaged

Introduction

The measured intensity I_d at each pixel of a harmonically vibrating object observed with an imaging interferometric device such as an ESPI or shearography system can be described by:

$$I_d = I_B + I_M \cos\varphi . J_0(\varphi_d), \text{ with } \varphi_d = \frac{4\pi}{\lambda} d(x,y) \quad (1)$$

when the integration time of the acquisition system is much longer than the vibration period. Here the information of interest, the vibration amplitude d, is in the argument φ_d of the zero order Bessel function of the first kind J_0. I_B and I_M are background and modulation intensities respectively, and φ is phase difference between the two interfering beams. When the vibration amplitude is zero, the value of the Bessel function is 1, and the intensity is given by the equation for the static case:

$$I_s = I_B + I_M \cos\varphi \quad (2)$$

This method is often referred to as the "time-averaged" method [1,2,3,4], and is relatively simple to implement, compared to other approaches, requiring pulse lasers, in many cases synchronized to the vibration, to "freeze" the motion of the vibrating object [5,6,7]. The usual method to obtain vibration fringe patterns is to acquire a series of phase-stepped interference patterns, usually four that are $\pi/2$ phase-stepped, producing intensities I_1 to I_4:

$$I_{d1} = I_B + I_M \cos\varphi . J_0(\varphi_d) \quad (3a)$$
$$I_{d2} = I_B - I_M \sin\varphi . J_0(\varphi_d) \quad (3b)$$
$$I_{d3} = I_B - I_M \cos\varphi . J_0(\varphi_d) \quad (3c)$$
$$I_{d4} = I_B + I_M \sin\varphi . J_0(\varphi_d) \quad (3d)$$

Eliminating the background intensity and phase, yields:

$$\sqrt{(I_4 - I_2)^2 + (I_3 - I_1)^2} = 2I_M|J_0(\varphi_d)| \quad (4)$$

For speckle-based measurement systems, the results are very noisy: since the nature of the modulation intensity is random, the term I_M causes considerable multiplicative noise on the Bessel modulated fringe patterns that contain the information of interest. Some improvement can be obtained by involving additional measurements taken in static conditions [4], but the nature of the fringe pattern remains the same: the vibration amplitude is an argument in the absolute value of a Bessel function. Sine-cosine filtering cannot be applied on the Bessel-type fringe pattern since filtering a pattern that is basically a speckle intensity pattern, would merely lead to larger speckles. Furthermore the results at zero crossings of the Bessel function would degrade when applying an averaging filter, because the derivative of its absolute value is not continuous there. Considerable improvements have been reached [8,9,10], also by involving measurements taken under stationary conditions, eliminating most of the noise and producing zero crossings and skeleton lines of a large number of Bessel-type fringes, allowing local inversion of the Bessel function. Regional inversion requires reliable skeleton indexing in order to be able to identify the correct fringe order for skeleton pairs. Inversion using look-up tables for each region is possible for most pixels in the vibration map when fringe density is high, leaving relatively small areas that cannot be inverted this way since their regions are limited only by one skeleton. For these pixels interpolation or even extrapolation is necessary. For low fringe densities these areas may be larger than the ones reported in Ref. [8]. Furthermore, discontinuities in the vibration field may adversely affect indexing causing inversion errors to propagate. Phase changes between the static and dynamic states are handled by level-shifting the phase iteratively, supported by histogram analysis [8,9,10]. In these references phase differences within the range of $-\pi$ to $+\pi$ are reported but no specific details on the level-shifts are given.

Another approach for quantitative evaluation of Bessel fringes is based on the acquisition of a series of speckle patterns with increasing vibration amplitude, followed by fitting the Bessel function as a function of vibration amplitude [11]. The Bessel function is approximated either by a cosine function with decaying amplitude for arguments larger than 1, requiring a sufficient number of data points in order not to miss fringe orders, and unwrapping of the cosine argument, or by a second degree polynomial for arguments smaller than 1. An advantage of this method is that it operates independently on single pixels, and therefore errors cannot propagate. A disadvantage is that a relatively large number of phase-stepped measurements have to be taken with different excitation settings. Furthermore, linearity between the excitation control parameters and the vibration amplitude is required. The approach relies on the assumption that no phase changes occur between the static and dynamic states.

Time-averaged vibration patterns may have much lower quality than the ones presented in Refs. [8] to [10], giving rise to the question whether patterns obtained outside the more or less stable conditions of the laboratory could render indexed skeletons that are reliable enough for regional inversion. In view of this we propose a method that produces reliable results even when the data sets have lower quality. In contrast with the approach followed in Ref. [11], only two sets of four phase-stepped interferograms, one set for the dynamic state, the other for the static one, are sufficient to produce acceptable results. The method operates on single pixels, or on a series of pixels within a given kernel, so errors do not propagate, avoiding problems at discontinuities in the vibration displacement map. It yields true Bessel-modulated vibration amplitude maps in a straight-forward manner when phase changes between the static and dynamic states can be neglected, and offers the option to correct for phase changes through an additional procedure, if necessary.

Linear regression for true Bessel-modulated vibration amplitude maps

The sign of the Bessel function can be retrieved when a set of steady state measurements, taken under the same conditions as the dynamic one, is available [10,11]. When this is the case, another set of equations (3), with $J_0(\varphi_d) = 1$, can be used to solve the unknowns I_B, I_M, and φ. The quantity of interest, $J_0(\varphi_d)$, can then be expressed in the measured intensities, while preserving the sign of the Bessel function. This approach only holds if there is no change in I_B, I_M, and φ between the static and dynamic states.

I_B can be eliminated from both the static and dynamic sets by subtracting Eq. (3b) from (3d) and (3c) from (3a), using subscript *s* for the static case:

$$I_{s4} - I_{s2} = 2I_M \sin\varphi \quad (5a)$$
$$I_{s1} - I_{s3} = 2I_M \cos\varphi \quad (5b)$$

Similarly using *d* as a subscript for the dynamic state we can write:

$$J_0(\varphi_d) = (I_{d4} - I_{d2})/2I_M \sin\varphi \quad (6a)$$
$$J_0(\varphi_d) = (I_{d1} - I_{d3})/2I_M \cos\varphi \quad (6b)$$

Substituting Eqs. (5a) and (5b) in (6a) and (6b) respectively yields:

$$J_0(\varphi_d) = (I_{d4} - I_{d2})/(I_{s4} - I_{s2}) \quad (7a)$$
$$J_0(\varphi_d) = (I_{d1} - I_{d3})/(I_{s1} - I_{s3}) \quad (7b)$$

The sign of the Bessel function is preserved, but the division may cause large errors when modulation I_M is in the order of the noise level. Division by zero due to zero-values of sine or cosine can be avoided by selecting the alternative equation, but zero-modulation, which can also be expected due to the nature of speckle patterns, has also to be dealt with.

An alternative method for processing vibration patterns yielding true Bessel-modulated vibration amplitude maps is proposed [12]. The method handles a relatively small number of low-order Bessel-type fringes and is based on linear regression. The method yields patterns where the vibration amplitude is an argument of a true Bessel function, not its absolute value. As a result, spatial frequencies of the Bessel-type fringe pattern are only half of those obtained with standard methods, and results can be filtered and normalized conveniently. The method is based on the notion that the intensity measured when the object of interest is vibrating harmonically can be written as a linear function of the intensity measured in the stationary state. This can be shown by substituting the term $I_M \cos(\varphi)$ from Eq. (2) into Eq. (1). If phase φ, background I_B and modulation I_M are the same for the static and dynamic case – which is not always the case, the dynamic intensity is given by:

$$I_d = J_0(\varphi_d) I_s + I_B(1 - J_0(\varphi_d)) \quad (8)$$

A series of intensity measurements taken under stationary conditions is now compared with the corresponding series for the dynamic case. For instance $\pi/2$ phase-stepping can be used to obtain four different intensity values for both cases; the resulting data pairs are then processed in a linear regression procedure for each pixel yielding the constant $J_0(\varphi_d)$ for the linear term in Eq. (8). Under the condition that I_B is the same for all data points, the constant term $I_B(1 - J_0(\varphi_d))$ is not relevant in the regression procedure.

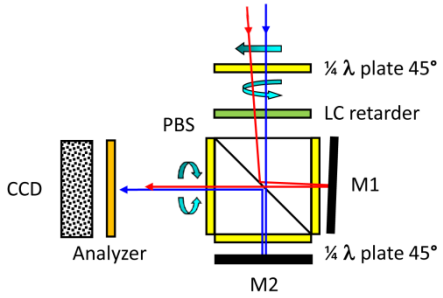

Figure 1: Subset of a LCR phase-stepped polarization-based shearing interferometer.

To evaluate the performance of existing and proposed methods some measurements have been taken on a vibrating object. The object was a Fokker 100 air brake with a free edge. This portion of the component consists of a thin Al plate, thickness 0.3 mm, supported by the relatively stiff structure of the brake on the left side, and vibrating freely at the right side. The object was excited by a loudspeaker on the backside, at a frequency of 147 Hz. The speckle interferometer used was a modified subsystem of an existing shearography system [13, 14]. The subsystem, a polarisation-sensitive shearing interferometer in Michelson configuration, is shown in Fig. 1. Basically, the optical subsystem causes two images of the object to interfere, taking care that the images are orthogonally polarised, and that one of them can be phase-stepped relative to the other. Temporal phase-stepping has been performed using a liquid crystal retarder, axis at 0°, positioned behind a quarter-wave plate oriented at 45°. The quarter-wave plate provides even distribution of the polarised optical energy entering the system. When the input beams have the same intensity and are linearly polarised with unknown polarisation direction, two orthogonally polarised beams with the same intensity leave the polarising beam splitter cube. A quarter-wave plate oriented at 45° at the exit of the beam splitter converts linear light leaving the beam splitter into two counter-rotating circularly polarised light beams, after which an analyser causes the two beams to interfere. Shearing is implemented by a small tilt of

mirror M1, effectuating interference between two points on the object at a single point on the sensor; the applied shear was in vertical direction. The imaging optics system is not shown in Fig. 1. All speckle patterns were acquired at a resolution of 512x512 pixels.

A result obtained by standard processing, using Eq. (4), is shown in Fig. 2a. Bessel-type fringes are visible, but fringe visibility is poor, as the Bessel term decreases with increasing amplitude. The absolute value of the Bessel fringes are shown. Compared to that, a result obtained using Eqs. (7a) and (7b) is shown in Fig. 2b.

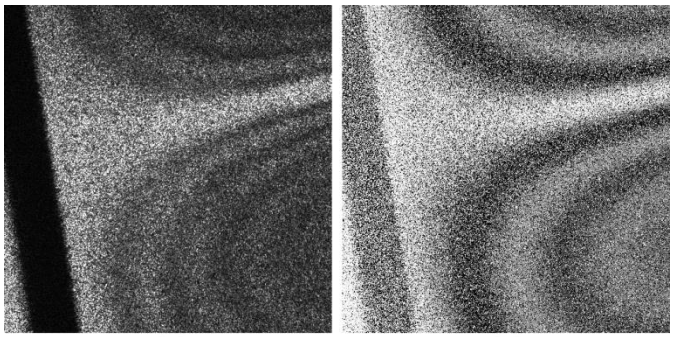

(a) (b)

Figure 2: Vibration pattern for a harmonically vibrating object at 147 Hz, a portion of a Fokker 100 air brake, measured with a shearography system, applying vertical shear. The dark area at the left side is not illuminated. (a) Standard processing. (b) Processing by solving J_0 directly from four phase-stepped equations acquired in the dynamic state, and 4 at steady state. Results truncated at 1.0 and –0.40276. Image size is 512x512 pixels.

While the sign of the Bessel function has been preserved using stationary data, the noise level of the resulting vibration pattern shown in Fig. 2b is extremely high. The vibration pattern shown in Fig. 2b could only be visualised after truncating the data at the known maximum and minimum of the Bessel function at 1.0 and –0.40278.

An indication of the quality of these results has been obtained by taking the standard deviation of the results in a limited region of the data field, after removing the average in that region, point by point. The average has been obtained from a high quality filtered version of the vibration pattern. An area with average values of the Bessel function between 0.8 and 1.0 was selected. Values of the standard deviation calculated this way for the conventional approach and the method using steady state data are 0.6640 and 7.8724 respectively.

A result obtained for the proposed method, based on linear regression, using Eq. (8), and using the same dynamic data set and a corresponding data set acquired in the stationary state, is presented in Fig. 3a, clearly showing the main advantage of the new method: the vibration pattern is now continuous, allowing filtering and scaling to the known extreme values of the Bessel function. The relevant spatial frequencies are only half of those obtained with the traditional approach. All linear regression calculations have been carried out using an existing algorithm [15].

The results of the regression procedure may contain high noise peaks, requiring some way of post-processing to visualise the results. For that purpose the data presented in Fig. 3a, and further results, have been truncated to the known extreme values of the Bessel function, 1.0 and –0.40276.

Noise can be reduced by involving more data points in the regression procedure, for instance by increasing the number of phase steps. There is no need to apply calibrated phase steps, as long as the phase steps are reproduced for the stationary and vibrating states. Results for 8 phase steps are presented in Fig. 3b, after truncation to the known minimum and maximum of the Bessel function. The reduction of the standard deviation is in the expected range: 0.6259 for four phase-steps, versus 0.4474 for eight.

Using the steady state data set, the sign of the Bessel function might be retrieved [10,11], and used to modify the conventional results shown in Fig. 2a. A continuous Bessel modulated vibration amplitude map is obtained this way, but the standard deviation for the region selected is not changed: it remains 0.6640 against 0.6259 for the proposed method, which is slightly better. The latter however has greater potential for improvement by increasing the number of data points either by including more phase steps, or spatially, as will be shown in the next sections.

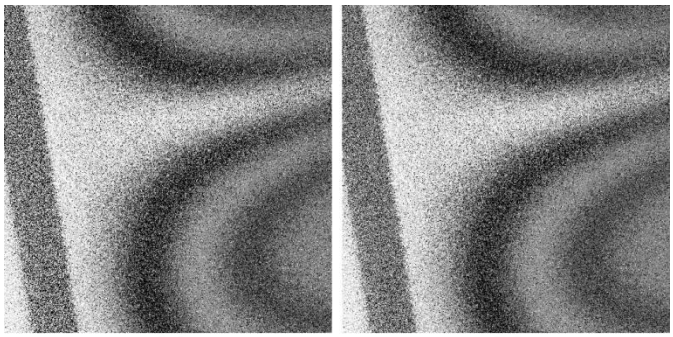

(a) (b)

Figure 3: Same object as in Fig. 2. Linear regression processing for single pixels, results truncated at 1.0 and –0.40276, (a) using four phase-steps, (b) using eight phase-steps.

In this section a comparison is made between noise reduction by spatial filtering and improving on the results by including all data points within the kernel used for spatial filtering in the linear regression procedure. The constant term $I_B(1 - J_0(\varphi_d))$ in Eq. (8) is not relevant in the regression procedure, if I_B is the same for all data points. This is only the case for single pixels, where the data are acquired in phase stepped intensity series. It would be interesting though to increase the number of data points for the regression procedure by combining pixel data in a neighbourhood around a central pixel. These pixels have different background intensities I_B, which must be eliminated before linear regression can be performed. This can be achieved by calculating the background intensity in the traditional way, but also by subtracting one of the phase-stepped speckle patterns given by Eq. (3) from the others in the same phase-stepped set. For instance, assuming a phase step of ϑ, subtraction of two patterns in the same set yields:

$$I'_S = I_M(\cos\varphi - \cos(\varphi + \vartheta)) \tag{9}$$

for the stationary state, and

$$I'_d = I_M(\cos\varphi - \cos(\varphi + \vartheta))J_0(\varphi_d) \tag{10}$$

for the vibrating state.

Substituting $I_M(\cos\varphi - \cos(\varphi + \vartheta))$ from Eq. (9) into Eq. (10) yields:

$$I'_d = J_0(\varphi_d)I'_s \tag{11}$$

Again a linear equation is obtained, suitable for linear regression, but now without a constant term. By subtracting the intensity values of one of the phase-stepped interferograms in a set from each of the other ones in that set, I_B is effectively eliminated from the data, and the neighbouring pixels, obtained from the same speckle pattern can be combined. Also pixels obtained from uncorrelated speckle interference patterns, for instance by using different illuminations, but acquired under the same vibration conditions, can be combined.

Three different kernel sizes have been used to compare results obtained for single pixels using Eq. (8), followed by averaging over the kernel, with an approach combining all data points in the kernel in a single regression procedure, using Eq. (11).

The results are presented in Fig. 4, for vibration patterns either spatially filtered or processed directly in kernels of 3x3, 9x9 and 15x15. The top bar presents standard deviation for linear regression processing using four phase-steps, on a single pixel. The results for the three different kernels are grouped in sets of three: the top bar of each set represents the standard deviation that would be obtained in conformance with a reduction with a factor of $\sqrt{n}$; the second bar shows the results for spatial averaging, and the third one for the linear regression procedure including all pixels in the kernel.

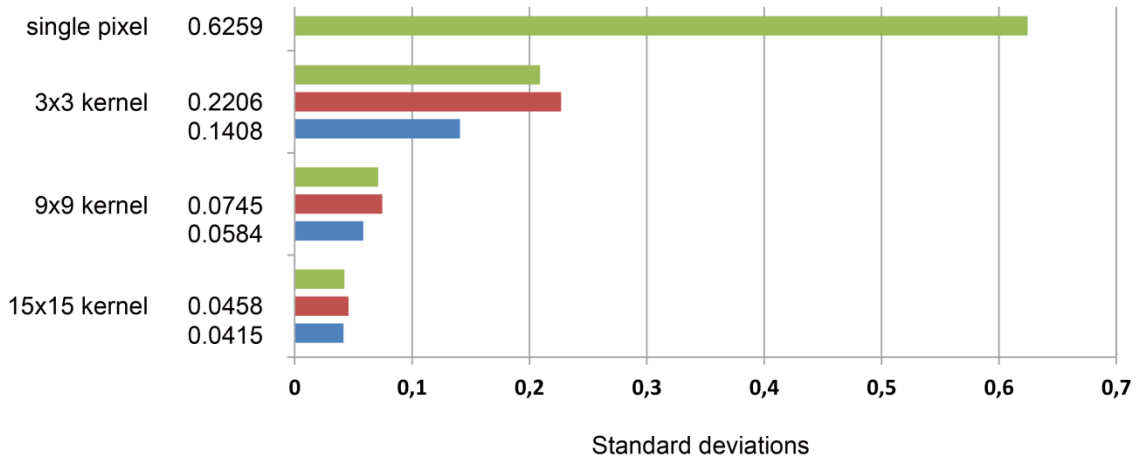

Figure 4: Standard deviations for linear regression processing using four phase-steps. Comparison between single pixel processing followed by averaging in three different kernels, with linear regression processing over the full kernel. For each kernel three results are presented: top bar, expected result based on a reduction with a factor of $\sqrt{n}$, second and third bar results for spatial averaging and linear regression processing over the full kernel.

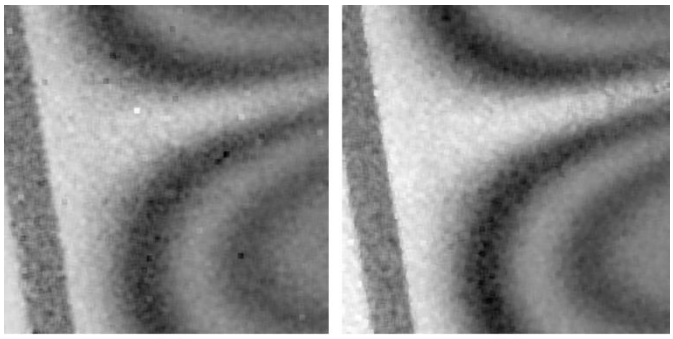

Figure 5: Same object as in Fig. 2. Linear regression processing using four phase steps, (a) after an averaging filter of 9x9, (b) combining pixels in a 9x9 neighbourhood.

Fig. 5 shows one of the compared results: in Fig 5a the vibration pattern spatially filtered using a kernel of 9x9 is shown. In comparison Fig. 5b shows the pattern obtained by processing all of the data points in the kernel in a single regression procedure. Results are shown truncated at the known extremes of the Bessel function.

When comparing these results it appears that noise reduction by spatial filtering, represented by the reduction of the standard deviation, is slightly less than what might be expected from the increase of the number of data points involved, for all kernels investigated.

The regression procedure shows better results, up to kernels of 9x9. As kernels are larger, the differences get smaller. The strongest gain has been observed for the smallest kernel of 3x3; it shows a better result than might be expected from the increase of data points: 0.1408 against 0.6259/3 = 0.2086. The rapid initial decrease of the standard deviation for processing over increased kernel sizes can be explained by the assumption that initially, as more pixels get involved, the available data are distributed gradually over the full modulation range. This effect decreases for larger kernels, when the full modulation range is covered already. Based on these figures, we conclude that applying linear regression over a full kernel can replace spatial filtering effectively, especially for small kernels.

Another comparison that can be made is between the reduction of the noise levels when increasing the number of phase steps and the results obtained when performing linear regression over a kernel. Increasing the number of phase steps will not improve results significantly for pixels where modulation is low, while involving all pixels within a given kernel allows pixels with low modulation to be combined with pixels with higher modulation. Nevertheless, the standard deviation for the increase of phase steps with a factor of 2

reduces from 0.6259 for four phase-steps, to 0.4474 for eight. The results for the 3x3 kernel procedure outperform the $\sqrt{n}$ expectation for the 3x3 kernel procedure, as shown above.

The number of data points used for linear regression can also be increased by combining the data of a series of measurements using uncorrelated speckle patterns, by changing the illumination for each series. This is the speckle averaging variant of the linear regression method. The averaging method is equivalent to combined processing of all pixels in a kernel, when speckle size is in the order of pixel size. Two cases are compared: processing pixels in a 3x3 kernel, compared to processing a single pixel applying 9 independent illuminations. A similar result would be expected for both versions of speckle averaging if the 9 illuminations were truly independent. This seems not to be the case: correlation coefficients for the acquired speckle patterns, compared for the different illuminations, ranged from 0.30 to 0.50. Consequently the standard deviation for the 9 illuminations is only 0.2576 where 0.1408 was reached for the 3x3 kernel case. The assumption that the 9 illuminations are only partly independent is also supported by the results of conventional speckle averaging over 9 illuminations, using Eq. (4). The standard deviation for the result of this test was 0.4757, compared to 0.6640 for the single set, where a reduction with a factor of 3 was expected.

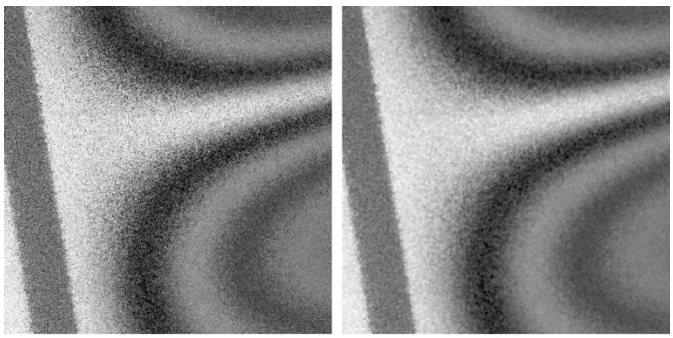

Figure 6: Same object as in Fig. 2. Linear regression processing using 8 phase steps, for 9 different illuminations (a) for single pixels, (b) combining pixels in a 3x3 neighbourhood.

An example of the result that can be reached when all available data for a single pixel are included is shown in Fig. 6a, where results are presented when 9 independent illuminations are used, and the number of phase steps is increased to 8. For these conditions, the standard deviation was 0.2563, less than could be expected from the increased number of data points involved. The total number of data points for Fig. 6a is 9x8 = 72, derived from 72 images for the static state and 72 for the dynamic one. This is an increase of a factor of 18 compared to the four phase-steps, single-pixel case, The expected improvement for the standard deviation with a factor of $\sqrt{18}$ is not reached for this speckle averaging case. The explanation for this is according to the one given above: the effectiveness of increasing the number of phase steps is limited, and speckle averaging over the 9 illuminations did not follow the $\sqrt{n}$ expectation.

When increasing the environment to 3x3 pixels the results shown in Fig. 6b are obtained. For these conditions, the standard deviation was 0.0891; compared to the case above, the reduction is slightly less than the expected factor of 3.

The examples presented in Fig. 4 show that including more data points in the linear regression procedure by extending the spatial range from which the data are taken is a feasible alternative for post processing using spatial filtering. For smaller kernels, up to 9x9, this approach outperforms spatial filtering. When including data acquired with uncorrelated speckle patterns a similar expected reduction has not been observed, caused by the fact that the applied different illuminations were only partly independent.

The results obtained can be demodulated using known image processing methods for indexing the Bessel fringes, followed by separating and indexing areas that are showing either monotone increasing or decreasing values. The argument of the Bessel function can then be obtained in each of these areas by separate look-up operations.

Correction for phase differences between stationary and vibrating states

Due to air turbulence or other disturbances, phase changes $\Delta\varphi$ between the measurements in the stationary and vibrating states may occur. This has an adverse effect on the results, as can be seen in Fig. 7a. The

distortions in the vibration pattern are related to phase changes occurring for that experiment, as shown in Fig. 7b, and sine-cosine filtered using a 25x25 kernel in Fig.7c.

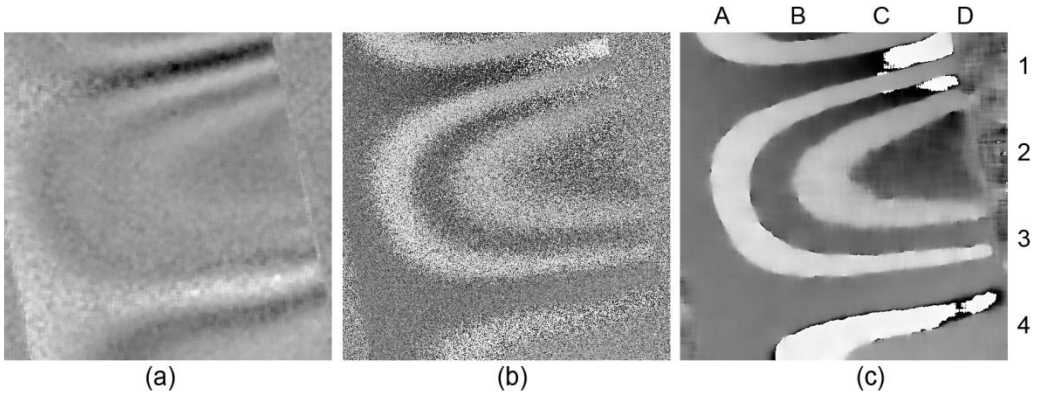

Figure 7: Same object as in Fig. 2, using four phase steps, combining pixels in a 9x9 neighbourhood. (a) degraded result due to phase difference between the stationary and vibrating states; (b) phase difference calculated with the standard four-bucket algorithm, (c) phase difference sine-cosine filtered using a 25x25 kernel.

The measured intensities in the vibrating state can be corrected for the phase change using the well-known equations for expressing sine and cosine of summed arguments (α, β) into the product of sine and cosine of the single arguments.

After correcting the measured intensities of a four-bucket phase-stepped dataset for the background, the corrected quantities are proportional to either the sine or cosine of the optical phase φ. For the stationary state we have:

$$I^*_{1s} = I_{1s} - I_B = I_M \cos\varphi \quad (12a)$$
$$I^*_{2s} = I_{2s} - I_B = -I_M \sin\varphi \quad (12b)$$
$$I^*_{3s} = I_{3s} - I_B = -I_M \cos\varphi \quad (12c)$$
$$I^*_{4s} = I_{4s} - I_B = I_M \sin\varphi \quad (12d)$$

and for the intensities measured in the vibrating state:

$$I^*_{1d} = I_{1d} - I_B = I_M \cos(\varphi + \Delta\varphi) J_0(\varphi_d) \quad (13a)$$
$$I^*_{2d} = I_{2d} - I_B = -I_M \sin(\varphi + \Delta\varphi) J_0(\varphi_d) \quad (13b)$$
$$I^*_{3d} = I_{3d} - I_B = -I_M \cos(\varphi + \Delta\varphi) J_0(\varphi_d) \quad (13c)$$
$$I^*_{4d} = I_{4d} - I_B = I_M \sin(\varphi + \Delta\varphi) J_0(\varphi_d) \quad (13d)$$

When $\Delta\varphi$ is 0, the linear regression procedure yields correct results, when not, the sine and cosine terms require correction. For the linear regression procedure the set needed would be:

$$I^*_{1d} = I_M \cos\varphi J_0(\varphi_d) \quad (14a)$$
$$I^*_{2d} = -I_M \sin\varphi J_0(\varphi_d) \quad (14b)$$
$$I^*_{3d} = -I_M \cos\varphi J_0(\varphi_d) \quad (14c)$$
$$I^*_{4d} = I_M \sin\varphi J_0(\varphi_d) \quad (14d)$$

However, the actual measurement is taken according to Eq. (13). To correct for the phase difference, we write $\cos\varphi$ and $\sin\varphi$ as:

$$\cos\varphi = \cos((\varphi + \Delta\varphi) - \Delta\varphi) = \cos((\varphi + \Delta\varphi)\cos\Delta\varphi + \sin(\varphi + \Delta\varphi)\sin\Delta\varphi \quad (15)$$
$$\sin\varphi = \sin((\varphi + \Delta\varphi) - \Delta\varphi) = \sin((\varphi + \Delta\varphi)\cos\Delta\varphi - \cos(\varphi + \Delta\varphi)\sin\Delta\varphi \quad (16)$$

using trigonometric relations for summed arguments of sine and cosine functions and with $\alpha = \varphi + \Delta\varphi$ and $\beta = \Delta\varphi$.

Eqs. (14a) to (14d) can then be written as:

$$I^*_{1d} = I_M \cos(\varphi + \Delta\varphi)\cos\Delta\varphi J_0(\varphi_d) + I_M \sin(\varphi + \Delta\varphi)\sin\Delta\varphi J_0(\varphi_d) \quad (17a)$$

$$I^*_{2d} = -I_M \sin(\varphi + \Delta\varphi)\cos\Delta\varphi\, J_0(\varphi_d) + I_M \cos(\varphi + \Delta\varphi)\sin\Delta\varphi J_0(\varphi_d) \quad (17b)$$
$$I^*_{3d} = -I_M \cos(\varphi + \Delta\varphi)\cos\Delta\varphi\, J_0(\varphi_d) - I_M \sin(\varphi + \Delta\varphi)\sin\Delta\varphi J_0(\varphi_d) \quad (17c)$$
$$I^*_{4d} = I_M \sin(\varphi + \Delta\varphi)\cos\Delta\varphi\, J_0(\varphi_d) - I_M \cos(\varphi + \Delta\varphi)\sin\Delta\varphi J_0(\varphi_d) \quad (17d)$$

The sine and cosine terms measured in the four-bucket dynamic dataset according to Eq. (13) can now be substituted into the corrected set given by Eq. (17).

Substituting Eq. (13a) and (13b) into Eq. (17a) yields:

$$I^*_{1d} = (I_{1d} - I_B)\cos\Delta\varphi - (I_{2d} - I_B)\sin\Delta\varphi \quad (18a)$$

The other three phase stepped measurements for the dynamic case can be corrected similarly:

$$I^*_{2d} = (I_{2d} - I_B)\cos\Delta\varphi - (I_{3d} - I_B)\sin\Delta\varphi \quad (18b)$$
$$I^*_{3d} = (I_{3d} - I_B)\cos\Delta\varphi - (I_{4d} - I_B)\sin\Delta\varphi \quad (18c)$$
$$I^*_{4d} = (I_{4d} - I_B)\cos\Delta\varphi - (I_{1d} - I_B)\sin\Delta\varphi \quad (18d)$$

The dynamic data set can be corrected for phase changes between the static and dynamic states using Eq. (18), containing measured intensities, the background I_B, that can be calculated as the average of the four measured intensities, and the phase change $\Delta\varphi$ that has to be determined. When the phase change is known, the corrected dynamic intensities can be processed with the measured static data set using a linear equation of the type given in Eq. (11).

Measuring the phase change between the stationary and vibrating states

The phase change between the stationary and vibrating states can be obtained in the conventional manner by applying the four phase-stepped equations (Eqs. (3a) to (3d)) to calculate phase for both the stationary state, with $J_0(\varphi_d) = 1$, and the vibrating state, or by using a direct method to obtain phase, involving all eight intensity measurements in one equation [16].

Both methods yield phase difference by using a four-quadrant inverse tangent function with sine and cosine arguments. However, at locations where the vibration amplitude is such that the argument of the Bessel function causes it to be negative, the inverse tangent from which phase is calculated for the dynamic case yields a result in the opposite quadrant, compared to adjacent regions where the Bessel function is positive: the value of the phase in areas where the Bessel function is negative differs by a value of π from the value obtained for areas with a positive Bessel function value [8]. Furthermore, the phase difference distribution may also contain 2π jumps when phase difference exceeds the $[-\pi, \pi]$ range. An example of such a pattern can be seen in Fig. 7b and 7c, showing both phase jumps of π and of 2π, unfiltered and sine-cosine filtered.

A way to avoid this situation is to calculate phase difference not by applying a two-argument inverse tangent function, but a single-argument one instead, yielding a phase range of $[-\pi/2, \pi/2]$ and phase jumps of π. Phase jumps of π, appearing at the zero crossings of the Bessel function, are not visible anymore since the calculation only covers two quadrants, and the single-argument inverse tangent is repeating modulo π. This distribution can be unwrapped by a dedicated method that can handle π steps, or by multiplying it by a factor of 2, causing the sine and cosine of the obtained distribution to be continuous at the 2π phase jumps. This allows sine-cosine filtering and subsequent unwrapping by any appropriate phase unwrapping method handling 2π phase jumps. The unwrapped phase difference distribution is then divided by a factor of 2 to obtain the desired distribution that is needed for the correction. After unwrapping the phase difference map a decision has to be taken whether or not a correction of π has to be added, depending on the starting point for the unwrapping procedure, in view of the fact that the wrapped distribution is available only in the $-\pi/2$ to $+\pi/2$ range.

The method has been tested using a modeled data set: the sine and cosine of the phase distribution of a modeled speckle field was modulated by a smooth Bessel-type fringe pattern. Phase noise of $\pi/8$ was added to the 4-bucket data set for the vibrating state. The unmodified speckle field served as the stationary set. To simulate a phase change between the stationary state and the vibrating state a linear phase change running from $-\pi$ to $+\pi$, including phase noise of $\pi/8$ was added to the dynamic set. The results are shown in Figs. 8 and 9. Fig. 8a shows the phase change, Fig. 8b and Fig. 8c present phase difference obtained with the two-argument and single-argument inverse tangent calculations respectively. Fig. 8b shows a central 2π wrapping only in the π-shifted regions, not in the regions with positive values of the Bessel function, as expected. In Fig. 8c all π wrappings connected with the positive and negative Bessel values have

disappeared, but the 2π phase difference distribution applied for the model now shows two phase jumps from $-\pi/2$ to $+\pi/2$. This wrapped distribution can be easily unwrapped by first multiplying it with a factor of 2, then applying a sine-cosine filter, and finally, after unwrapping, dividing it again by a factor of 2. The result, a smooth phase difference distribution, could then be used to correct the dynamic data set according to Eqs. (18a) to (18d), followed by linear regression processing using a linear equation of the type given in Eq. (11).The results are shown in Fig. 9, the degraded vibration pattern in Fig. 9a, and a corrected pattern in Fig. 9b.

Figure 8: (a) Simulated phase difference running from $-\pi$ to $+\pi$, $\pi/8$ noise added. (b) Phase difference for a simulated vibration pattern, calculated with a two-argument inverse tangent. (c) same as (b), calculated with a single-argument inverse tangent.

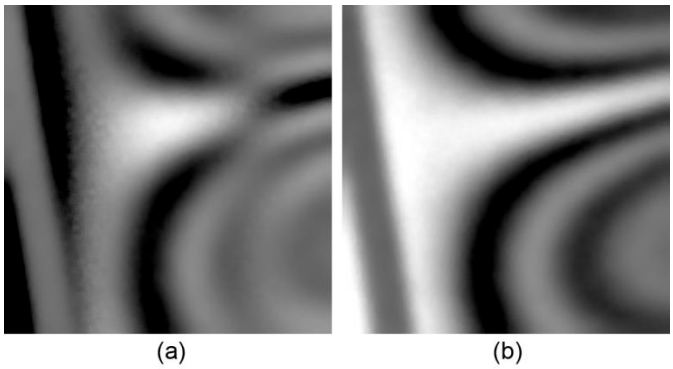

Figure 9: Modeled vibration pattern, (a) degraded, due to a $-\pi$ to $+\pi$ phase difference between the stationary and vibrating states and (b) vibration pattern after correction.

Success of the method mainly depends on the capability of the unwrapping method to unwrap the phase difference map in the $[-\pi/2, \pi/2]$ range in the presence of noise and singularities. The relative noise level for that distribution is twice as large compared to the wrapping values of that map than would be the case in a $[-\pi, \pi]$ range. Because the noise level for our experimental data, for which a degraded result was shown in Fig. 7a, was too high for our unwrapping facilities to be successful, a second approach has been followed that could handle our experimental data.

The second method is based on the identification of areas in the vibration pattern where the vibration displacement is such that the Bessel function has negative values. When observing the pattern it is clear where that is the case, but for an image processing system it is less obvious, the algorithm may have to deal with both π and 2π wrappings, as can be seen in Figs. 7b and 7c, showing the unfiltered and 25x25 sine-cosine filtered phase difference maps, calculated with the standard two-argument inverse tangent function. The presence of 2π phase jumps prevents the use of a relatively simple approach applying a threshold to separate the regions with positive and negative values of the Bessel function [8]. The approach chosen to achieve the desired objective is to divide the image – and thus the problem – into a series of smaller ones, and to use the distribution of the data in each sub-image to decide on how large a level shift of the local phase in the sub-image would be necessary to arrive at the situation that no 2π phase jumps occur in the sub-image. The procedure may consist of a limited number of iterations, each iteration with a sub-image size reduced by a factor of two. We used only one, handling 16 sub-images. The area over which the histograms

are taken for the first iteration, should be large enough to cover fringes in both regions, positive and negative.

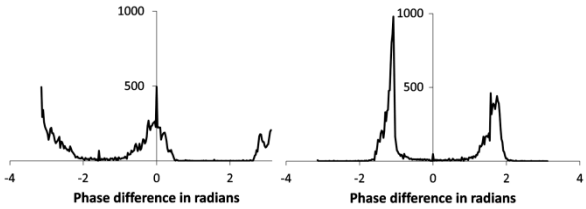

Figure 10: Local histograms of phase difference distribution, shown in Fig. 7c. (a) Local area C1 and (b) Local area A2.

A 2π phase step in either one of both regions is characterized by three peaks in the histogram: one at $-\pi$, and another one at $+\pi$. The third region is represented by a third peak, around 0 (Fig. 10a). In such a situation the algorithm decides that either a positive or negative shift of $\pi/2$ has to be applied to remove the wrapping while preventing that one appears in the other region. This choice actually implies a decision on which region corresponds with positive values of the Bessel function. The decision can only be taken when the boundary conditions are taken into consideration: both possibilities are checked for the mismatch they cause with the boundary pixels of the sub-image previously processed. A safe sub-image to start with is a sub-image for which the regions are known, requiring only a small or at least a known shift to provide an acceptable starting condition.

The algorithm also handles situations where no 2π phase jumps are present in a sub-image. Those situations are characterized by the presence of only two peaks in the histogram, representing the positive and negative regions, or by a single one (Fig. 10b). In case there are two peaks, the peak representing the highest number of occurrences is shifted to either $-\pi/2$ or to $+\pi/2$, depending again on the boundary conditions. The level-shifted state can be used to separate the regions with positive and negative Bessel function values. Applying a threshold at 0 yields a binary result to serve as a mask for the correction of π in the initial phase difference map, for regions where the value of the Bessel function is negative.

Results for an experimental data set, as shown in Fig. 7, with a large phase difference between the stationary and vibrating states, exceeding the $[-\pi,+\pi]$ range, are shown in Figs. 11 to 13. Fig. 11a shows the phase difference, after local level shifting in 4x4 sub-images, succeeding to remove 2π phase jumps, and approaching a more even phase difference distribution, suitable for applying a threshold to obtain a mask. The 16 level shifting data points have been re-sampled into the original size of the phase difference map and subtracted from the original filtered one, with wrappings. The result is shown in Fig. 11b. The mask is shown in Fig. 11c.

Figure 11: Phase difference map. (a) locally level-shifted in 16 sub-mages, (b) phase difference in Fig. 7c corrected using resampled level shift data, (c) mask obtained by applying a threshold on (a), and 5x5 filtered.

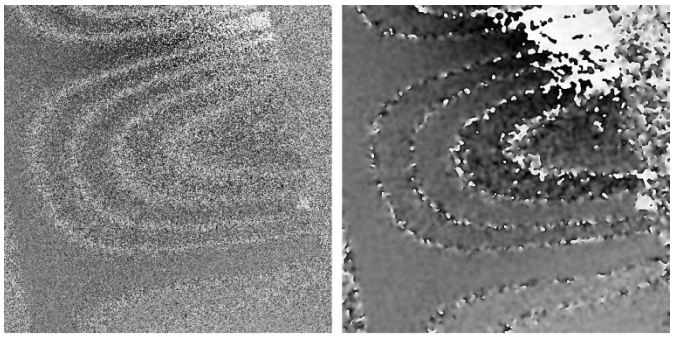

(a) (b)

Figure 12: Phase difference in Fig. 7b corrected by adding π to the bright areas in the mask shown in Fig. 10c (a) unfiltered, and (b) 25x25 sine-cosine filtered.

The mask has been used to correct the unfiltered phase difference, shown in Fig. 7b, adding an amount of π to the areas with negative Bessel function values. The result is shown in Fig 12a, and 25x25 sine-cosine filtered in Fig. 12b. The corrected phase difference still shows the presence of the zero Bessel crossings, and would be hard to unwrap, but that is not necessary: the correction procedure only uses sine and cosine, which are continuous at 2π phase jumps.

After determining phase difference between the static and dynamic states, the intensity values for the dynamic state can be corrected using Eq. (18) and processed together with the measured static data set using a linear equation of the type given in Eq. (11). The final corrected vibration pattern is presented in Fig. 13b, together with the uncorrected pattern, in Fig. 13a. Both patterns have been obtained by the linear regression procedure using four phase steps, combining the data in an environment of 9x9 pixels.

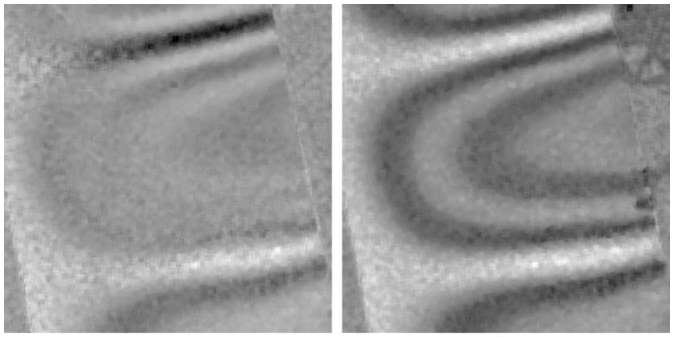

(a) (b)

Figure 13: Vibration pattern, obtained by linear regression processing using four phase steps, for an experiment with phase difference exceeding the $-\pi$ to $+\pi$ range. Pixels in a 9x9 neighbourhood are included. (a) uncorrected, identical to Fig. 7a, and (b) corrected.

Discussion and Conclusions

A new method for processing time-average vibration patterns measured with a speckle interferometer using linear regression is proposed. Unlike conventional methods the proposed method yields true Bessel modulated vibration amplitude maps, instead of the absolute value of the Bessel function.

The vibration patterns produced contain only half the spatial frequencies compared with conventional methods, and are continuous at zero crossings of the Bessel function. The patterns can therefore be filtered conveniently and scaled to the known extremes of the Bessel function. The results provide a useful starting point for complete demodulation of the Bessel modulated vibration amplitude distribution.

The proposed method uses additional information from the stationary state and is based on the notion that the phase stepped intensity during the vibration can be written as a linear function of the stationary intensity.

Extreme values of the Bessel function resulting from the linear regression procedure can be truncated to the known extremes of the Bessel function: –0.40267 and 1.0 respectively. This is useful for visualizing the data.

The proposed linear regression method offers an option to reduce the noise level by involving a sufficient number of data points, either spatially or by taking more phase steps. Increasing the number of phase steps from 4 to 8 reduces the standard deviation with a factor in correspondence with the $\sqrt{2}$ expectation. The method also supports speckle averaging: the combination of measurements taken with independent speckle patterns in a single regression procedure. Speckle averaging did not bring the expected reduction of the standard deviation for the available dataset using 9 different illuminations, due to the fact that the illuminations were not completely independent.

Kernel-based speckle averaging in a kernel of 3x3 outperforms the $\sqrt{9}$ expectation, most likely caused by the fact that the increased dataset may cover a larger portion of the modulation range, which is not the case when the number of phase steps is increased. Kernel-based speckle averaging proves to be very effective for kernels of modest size, better than spatial filtering, up to kernels of 9x9 pixels.

Phase differences between measurements taken in the static and dynamic states cause degradation of the results. These differences can be successfully corrected involving the sine and cosine of the phase difference.

Two methods to quantify the differences have been used: the first one was based on calculation of phase differences using the single-argument inverse tangent followed by unwrapping. The applicability of this method relies on the capability of the unwrapping procedure to handle noise and singularities in the phase difference map.

The second method is based on identification of regions within the vibration pattern with positive and negative values of the Bessel function. The identification process uses local level shifting of phase differences, based on histogram analysis, eliminating 2π phase jumps, allowing the application of a reliable threshold to produce a mask that can be used to correct the phase difference distribution.

The linear regression method only requires two phase-stepped series of data to be available, one for the stationary state, the other for the vibrating state. It is not necessary for the phase steps to be known, but they should be the same for both states. The correction procedure for phase differences however does require phase difference to be known, implying that the phase steps must be known. This is true in most cases, but not all, for instance not when quadrature phase-stepping is applied. In that case phase difference can also be calculated without knowing the temporal phase steps [14].

The approach using linear regression has high numerical stability, provided that the matrix inversion software involved is protected against the occurrence of a singular matrix. Errors cannot propagate since the linear regression procedure is performed locally.

References

1. Tiziani, H.J. (1978) Vibration analysis and deformation measurement. *Speckle metrology*, Erf, R.K., editor, Academic Press, New York.
2. Slettemoen, G. A. (1980) Electronic speckle pattern interferometric system based on a speckle reference beam. *Applied Optics* Vol. **19**, No. 4, 616-623.
3. Nakadate, S. (1986) Vibration measurement using phase-shifting time-average holographic interferometry. *Applied Optics* Vol. 25, No. 22, 4155-4161.
4. Vikhagen E. (1989) Vibration measurement using phase shifting TV-holography and digital image processing. *Opt Commun*.69(3,4):214–8.
5. Anderson, D.J, Valera, J.D. and Jones, J.D.C. (1993) Electronic speckle pattern interferometry using diode laser spectroscopic illumination. *Meas. Sci. Technol.* **4**, 982-987.
6. Pedrini, G. and Tiziani, H.J. (1997) Double pulse electronic speckle interferometry for vibration analysis. *Applied Optics* Vol. **36**, No. 22, 5310-5316.
7. Somers, P. A.A.M. and Bhattacharya, N, (2010) Vibration phase-based ordering of vibration patterns acquired with a shearing speckle interferometer and pulsed illumination. *Strain*, Vol 46, Issue 3, pp. 234-241, on-line 2008.
8. Borza, D. N. (2006) Full-field vibration amplitude recovery from high-resolution time-averaged speckle interferograms and digital holograms by regional inverting of the Bessel function. *Optics and Lasers in Engineering* 44 747–770.
9. Borza, D. N. (2002) A new Interferometric Method for Vibration Measurement by Electronic Holography. *Experimental Mechanics*, Vol . 42, No. 4, pp. 432-438.
10. Moreau, A.N, Borza, D. and Nistea, I. (2008) Full-Field Vibration Measurement by Time-Average Speckle Interferometry and by Doppler Vibrometry – A comparison. *Strain*, Vol 44, pp. 386-397.

11. Krzmien, L. and Lumomski, M. (2012) Algorithm for automated analysis of surface vibrations using time-averaged digital speckle pattern interferometry. Applied Optics, vol. 51, No. 21, pp. 5154-5160.
12. Somers, P.A.A.M. (2015) Processing time-average vibration patterns using linear regression, *Looking Beyond the Surface, Photomechanics 2015,* pp 70-71.
13. Somers, P.A.A.M. and Bhattacharya, N. (2007) , "Handling unfavourable polarization states in a polarization-based shearing speckle interferometer", J. Opt. A: Pure Appl. Opt. 9, S92-S97.
14. Somers, P.A.A.M. and Bhattacharya, N. (2006) Three-bucket quadrature phase stepping in a shearing speckle interferometer**,** *Speckle06 Proceedings: Speckles, from Grains to Flowers*, *Proceedings of SPIE*, Vol. 6341, pp. 63411K-1 - 63411K-6, Pierre Slangen, Christine Cerruti eds.
15. Press, W.H, Teukolsky, S.A, Vetterling, W.T. and Flannery, B.P. (1997) *Numerical Recipes in C*, 2nd ed. Cambridge University Press, Cambridge.
16. Creath, K. (1994) Phase-Shifting Holographic Interferometry, *Holographic Interferometry*, ed. P.R. Rastogi, Springer Series in Optical Sciences, 68, 109-150, Springer-Verlag, Berlin